

## Damage prediction of RC containment shell under impact and blast loading

A.K. Pandey\*

Central Building Research Institute, Roorkee (CSIR), 247667, Uttarakhand, India

(Received December 13, 2009, Accepted August 22, 2010)

**Abstract.** There is world wide concern for safety of nuclear power installations after the terrorist attack on World Trade Center in 2001 and several other civilian structures in the last decade. The nuclear containment structure in many countries is a double shell structure (outer shell a RCC and inner a pre-stressed concrete). The outer reinforced concrete shell protects the inner shell and is designed for external loading like impact and blast. A comparative study of non-linear response of reinforced concrete nuclear containment cylindrical shell subjected to impact of an aircraft (Phantom) and explosion of different amounts of blast charges have been presented here. A material model which takes into account the strain rate sensitivity in dynamic loading situations, plastic and visco-plastic behavior in three dimensional stress state and cracking in tension has been developed earlier and implemented into a finite element code which has been validated with published literature. The analysis has been made using the developed software. Significant conclusions have been drawn for dissimilarity in response (deflections, stresses, cracks etc.) of the shell for impact and blast loading.

**Keywords:** impulsive; dynamic; blast charge; yielding; visco-plastic; tensile cracking.

---

### 1. Introduction

India has an ambitious target of constructing a number of reactors in near future as 123 Agreement with USA will ensure availability of supply of nuclear fuel for reactors. The safety of these nuclear power installations is a matter of concern in view of terrorist activity in the region. These special structures are required to be designed for impact and blast loads in addition to normal loads during their service life. The loading from impact and blast is often extreme loading with low probability of occurrence and therefore analysis has to be made till ultimate stages with more rational material models in-order to reduce the safety margins. Nuclear containment structure in many countries is composed of a pre-stressed containment shell with an outer reinforced concrete shell. The studies are reported in literature (Rebora *et al.* 1976, Crutzen *et al.* 1981, Cervera *et al.* 1987, Abbas *et al.* 1996, Kukreja 2005) for the impact of an aircraft on outer reinforced concrete nuclear containment shells, however studies are rarely reported (Pandey *et al.* 2006a) on the effect of explosions on the containment shells. Terrorist attacks on civilian structures have generated a lot of heat for study of public buildings subjected to impact and blast loading. Many studies are reported for full scale structures which have suffered explosions (Mlakar *et al.* 1999, Luccioni *et al.*

---

\*Corresponding author, Ph.D., E-mail: [akp\\_sed@rediffmail.com](mailto:akp_sed@rediffmail.com)

2004, Oстераas 2006). Hydrocodes are also being used (Luccioni *et al.* 2004, Gong *et al.* 2009) for blast simulation which requires a huge computational effort. Pressure loading and its interaction is more accurately predicted with hydrocodes but constitutive relationships for concrete and steel may need further refinement. The impact of aircraft attack on world trade center towers (WTC1 and WTC 2 which were steel structures have been studied (Omika *et al.* 2005) using LS-DYNA (hydro code) finite element software.

The rate of loading/straining is very high in impact and blasts compared to quasi-static situations and material properties of construction materials are loading rate dependent. The strain rate in such cases may vary from  $10^{-6}$ /sec. for the static case to 10 /sec for the case of blast loading. With the availability of dynamic experimental results on concrete and steel the material constitutive relations have undergone a fast improvement. Many strain rate dependent constitutive relationships have been

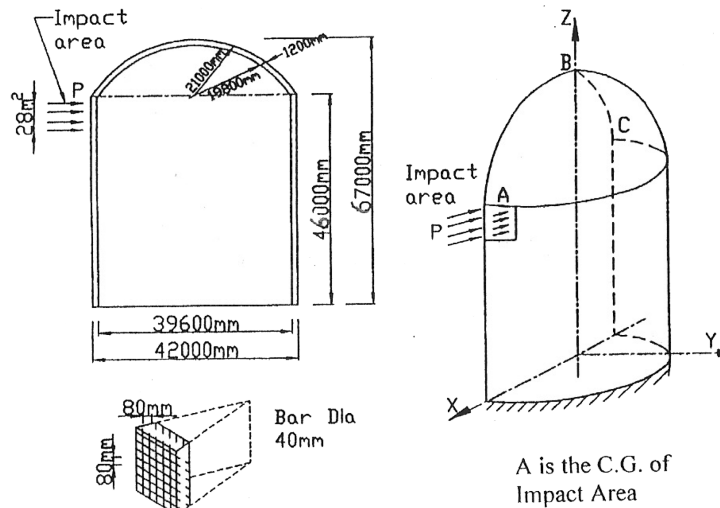


Fig. 1(a) General layout of the outer reinforced concrete nuclear containment shell

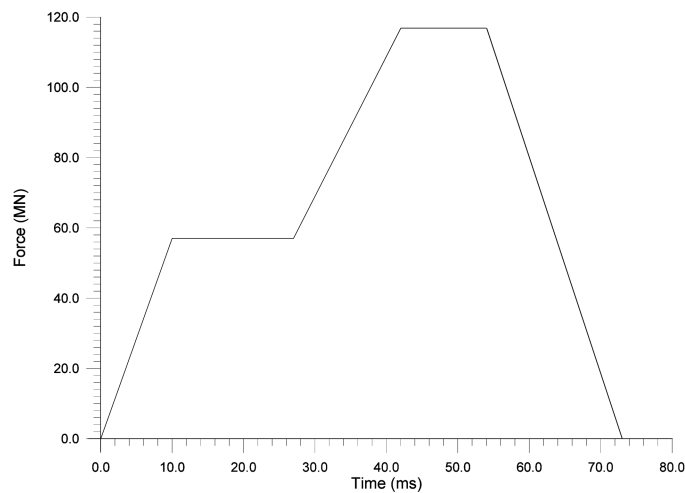


Fig. 1(b) Force time function for Phantom Aircraft

proposed in uniaxial compression (Scott *et al.* 1982, Dilger *et al.* 1984, Soroushian *et al.* 1986, Xiao *et al.* 2008), two dimensional loading situations (Ngo *et al.* 2009) and multiaxial loading situations (Nilsson *et al.* 1981, Bicanic *et al.* 1983, Yang *et al.* 2004, Pandey *et al.* 2006b). The material model (Pandey *et al.* 2006b) employed in the analysis here takes into account the pressure sensitive behavior of concrete in three dimensional loading situations and strain rate sensitive behavior in dynamic loading situations in a better way compared to earlier studies. The paper presents the study of reinforced concrete nuclear containment shell (Fig. 1(a)) for impact of Phantom aircraft (Fig. 1(b)) and blast pressures from explosions at close range and long range.

## 2. Finite element analysis

The finite element analysis of reinforced concrete containment shells under impact and blast loading requires proper choice of the element to model concrete and reinforcement realistically, numerical integration scheme to get required degree of accuracy and computational efficiency and most importantly appropriate non-linear material constitutive relationships to model the behavior. A material model considering strain rate dependent constitutive relationship for concrete and steel has been developed and implemented into finite element code named DYNAIB. The finite element code DYNAIB is a program for transient dynamic analysis using 20 noded iso-parametric brick element and steel layer is embedded in it with full strain compatibility between steel and concrete. After cracking concrete is assumed to be orthotropic and tension softening/stiffening curve is employed to represent the average behaviour and shear modulus is reduced depending upon the crack width. The non-linear material model employed in the formulation has been already published (Pandey *et al.* 2006b) and briefly described here.

### 2.1 Non-linear material modeling

Concrete is a pressure sensitive material and the material model adopted here takes into account the pressure sensitivity in three dimensional loading situations by adopting proper yield and failure surfaces as discussed below. The results of dynamic experiments (Atchley *et al.* 1966, Hughes *et al.* 1972, 1978, Dilger *et al.* 1984, Bischoff *et al.* 1991, Cadoni *et al.* 2000) on concrete have demonstrated that compressive, tensile and flexural strength depend upon the rate of loading. The strength and secant modulus of elasticity increase as the rate of loading increases however tangent modulus of elasticity is relatively unaffected. To study strain rate dependent behavior and pressure sensitivity of concrete in three dimensional loading conditions, material model based on elasto-viscoplasticity have been employed.

#### 2.1.1 Viscoplastic consideration

The non-linear behavior has been studied using the Perzyna's, 1966 theory of elasto-viscoplasticity. A generalized three-dimensional failure criterion for concrete by Menetrey and William (1995) has been implemented into a finite element code. The model adopted in the study includes strain rate effect at two levels, (i) The fluidity parameter varies as a function of strain rate (ii) The failure surface is function of dynamic strength which varies according to strain rate.

### 2.1.2 Perzyna's elastic-visco-plastic theory

The static yield condition expressed in the following form.

$$F(\sigma_{ij}) = f(\sigma_m, J_2, J_3) / \sigma_y - 1 \quad (1)$$

Where,  $f$  is a homogeneous function of stresses (three stress invariants) and  $\sigma_y$  is a scalar yield stress. As usual, the total strain can be separated in elastic and visco-plastic parts

$$\varepsilon_{ij} = \varepsilon_{ij}^e + \varepsilon_{ij}^{vp} \quad (2a)$$

The visco-plastic strain rate is given by

$$\dot{\varepsilon}_{ij}^{vp} = \gamma \langle \phi(F) \rangle \frac{\partial f}{\partial \sigma_{ij}} \quad (2b)$$

The function  $\langle \phi(F) \rangle$  has the following meaning.

$$\begin{aligned} \langle \phi(F) \rangle &= 0 \quad \text{if } f \leq f_y \\ \langle \phi(F) \rangle &= \phi(F) \quad f > f_y \end{aligned} \quad (2c)$$

$$\phi(F) = \frac{f(\xi, \rho, \theta) - f_y}{f_y} \quad (2d)$$

The function  $\partial f / \partial \sigma_{ij}$  is a direction component. The direction of visco-plastic strain rate is thus normal to the surface  $f = \text{constant}$ .  $f(\xi, \rho, \theta)$  and  $f_y$  are defined by Eqs. 3(a) and 3(b).

Thus, we have a complete stress-strain relation in the elastic range and only a differential law regarding the visco-plastic part of the strain in plastic range. Here,  $\gamma$  denotes a fluidity parameter having dimensions of  $(\text{time})^{-1}$ . The fluidity parameter has been obtained from available experimental data obtained from uniaxial stress-strain curves for concrete.

### 2.1.3 Yield and failure criterion

The three-parameter criterion (Menetrey and Willam 1995) adopted in the formulation is in principal stress space and is defined as

$$F(\xi, \rho, \theta) = f(\xi, \rho, \theta) - f_y = 0 \quad (3a)$$

$$F(\xi, \rho, \theta) = \left[ \frac{\sqrt{1.5}\rho}{f_{cd}} \right]^2 + m \left[ \rho \frac{r(\theta, e)}{\sqrt{6}f_{cd}} + \frac{\xi}{\sqrt{3}f_{cd}} \right] - c = 0 \quad (3b)$$

$$\text{Here, } \xi = I_1 / \sqrt{3}, \rho = \sqrt{2J_2} \text{ and } \theta = \frac{1}{3} \cos^{-1} \left( \frac{3\sqrt{3}J_3}{2J_2^{3/2}} \right)$$

$I_1, J_2, J_3$  are stress invariants,  $r(\theta, e)$  is an elliptical function,  $e$  is an eccentricity parameter which is a function of uniaxial and biaxial compressive strength,  $c$  and  $m$  are defined as follows.

$$c = 1, m = \left[ \frac{3(f_c^2 - f_t^2)}{f_c f_t} \right] \frac{e}{e + 1}$$

Linear elastic behaviour has been assumed in the analysis up to  $0.35f_c$  and elastic modulus and initial yield surface which began at  $0.35f_c$  is strain rate independent.

$f_{cd}$  is the dynamic compressive strength obtained from uni-axial tests expressed as a function of strain rate ( $\dot{\epsilon}$ )

The following expression (Soroushian *et al.* 1986) has been adopted to calculate the dynamic compressive strength of the material from its static compressive strength.

$$f_{cd}/f_c = A_0 + A_1 \log_{10}(\dot{\epsilon}) + A_2 (\log_{10}(\dot{\epsilon}))^2 \quad (3c)$$

Where,  $A_0 = 1.48$ ,  $A_1 = 0.16$ ,  $A_2 = 0.0135$  are suggested for concrete.

The geometric representation of the above defined yield and failure criteria in principal stress space is convex and smooth and characterized by two parabolic meridians and a deviatoric section that changes from a triangular to a circular shape with increasing confinement.

### 2.1.4 Fluidity parameter

Fluidity parameter has been obtained from experimental stress-strain curves at different strain rates. The following expression has been numerically integrated for each stress-strain curve to obtain the fluidity parameter corresponding to that stress-strain curve at that particular strain rate.

$$\gamma = \frac{\int d\dot{\epsilon}^{vp}}{\int \left( \frac{\sigma - \sigma_y}{\sigma_y} \right) dt} \quad (4a)$$

Based on the study, an expression for the fluidity parameter  $\gamma$  is proposed below obtained by curve fitting of the experimental results.

$$\gamma(\dot{\epsilon}) = \dot{\epsilon}_{ref} e^{c_0 + c_1 \log \frac{\dot{\epsilon}}{\dot{\epsilon}_{ref}}} \quad (4b)$$

Where,  $\dot{\epsilon}_{ref} = 10^{-6}$ ,  $c_0 = -0.533172$ ,  $c_1 = 0.880166$

### 2.1.5 Damage and material degradation

From the uniaxial tensile tests on concrete it is known that concrete is very weak in tension and cracking begins early (at strain of 0.00015 to 0.00020) after reaching its tensile strength. As demonstrated from experimental results from uni-axial compressive tests on concrete after yielding visco-plastic deformation begins and after reaching ultimate strength (approximately at a strain of 0.0020) softening regime begins. Damage here refers to tensile cracking as well as yielding and failure as predicted by failure criterion. During the analysis concept of material degradation has been introduced, when a Gauss Point crosses failure surface, ultimate strength is reduced as a function of viscoplastic work.

### 2.2 Cracking behavior

The primary cause of non-linearity in concrete is tensile cracking. The smeared crack model proposed considers the effect of tensile cracking by a change in the material properties of concrete by smearing the crack over the entire affected element. Tension stiffening effect resulting from an

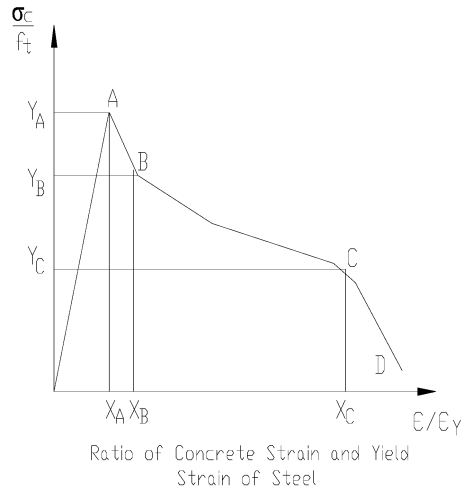


Fig. 2 Simplified effective tensile stress-strain curve (Gupta *et al.* 1990)

interaction between the cracked concrete and the reinforcement has been modeled as described below.

### 2.2.1 Model for tension stiffening effect

The model adopted for tension stiffening effect is based upon the tri-linear curve proposed by Gupta *et al.* (1990) based on theoretical studies, it is concluded that the tension-stiffening effect is a function of an area parameter, a bond parameter and a strength parameter. Parametric studies were performed to assess the effect of these parameters. Based on the theoretical studies, a  $\sigma$ - $\epsilon$  curve (Fig. 2) for concrete was proposed to include the tension stiffening effect in the post cracking phases. In the proposed curve, the  $X$ ,  $Y$  coordinates of the three control points  $A$ ,  $B$ ,  $C$  (Fig. 2) are determined by the following expressions.

$$X_A = \frac{nf_t}{f_{sy}} \quad Y_A = 1.0 \quad (5a)$$

$$X_B = \frac{nf_t}{f_{sy}} \left( 1 + \frac{1+n\rho_a}{10n\rho_a} \right) \quad Y_B = \left( 1 - \frac{1+n\rho_a}{10n\rho_a} \right) \quad (5b)$$

$$X_C = \left( 1 - \frac{nf_t}{2n\rho_a f_{sy}} \right) \quad Y_C = 0.5 \quad (5c)$$

Where  $n = E_s/E_c$  i.e., the modulus of elasticity ratio of steel to concrete,  $\rho_a$  is the area ratio of the reinforcement and concrete ( $A_s/A_c$ ),  $f_t$  is the tensile strength of concrete and  $f_{sy}$  is the yield strength of steel. Between the control points, an exponential curve is assumed which suitably simulates the experimental results.

### 2.3 Shear transfer across cracks

The behavior of the cracked concrete under shear stress is affected by the aggregate interlock, the

dowel action of the reinforcement across the crack and the axial stiffness of the reinforcing bars. There is thus still a transfer of shear stresses across the cracks but the shear modulus of concrete gets reduced on cracking. A simple expression for the reduced shear modulus has been used in the formulation.

$$G_c = \beta G_0 \quad (6a)$$

Where  $G_0$  is the shear modulus of the un-cracked concrete and  $\beta$  is a reduction factor varying from zero to one.  $\beta$  is related to the tensile strain normal to the crack plane is defined as

$$\beta = 1 - \left[ \frac{\varepsilon_t}{0.005} \right]^{k_1} \quad (6b)$$

Where  $\varepsilon_t$  is the tensile strain normal to the crack plane and  $k_1$  is a constant which may vary in the range of 0.3 to 1.0.

#### 2.4 Modeling for steel

The reinforcing steel has been assumed to have uni-axial properties in the direction of the bars. A elastoviscoplastic model has been used in the formulation where

$$\dot{\varepsilon}_{vps} = \pm \gamma(\dot{\varepsilon}_s) \frac{(\sigma_s - f_{sy})}{f_{sy}} \quad (7)$$

$$\gamma(\dot{\varepsilon}_s) = a_0 (\dot{\varepsilon}_s)^{a_1} \quad (8)$$

$\gamma(\dot{\varepsilon}_s)$  = fluidity parameter for steel as a function of strain rate

$\dot{\varepsilon}_{vps}$  = viscoplastic strain rate in steel

$\sigma_s$  = stress in steel,  $f_{sy}$  = yield stress in steel,  $a_0 = 1.539$ ,  $a_1 = 0.971$

### 3. Impact of phantom aircraft and blast of different amounts of charges on a containment shell

The geometry of the nuclear containment shell chosen for parametric studies is described in Fig. 1(a). The reinforced concrete shell is composed of cylindrical and spherical parts of uniform thickness. The cylindrical part is having an inner diameter of 39.6 m, outer diameter of 42.0 m, and height of 46.0 m. The reinforcement in the shell consists of bars of 40 mm diameter spaced 8 cm. c/c circumferentially and meridionally on the interior as well as exterior faces. Due to symmetry half of the shell has been discretized using 20 noded iso-parametric brick element (reduced integration with 15 Gauss Points) which has three translational degrees of freedom at each node. The half of the shell has been modeled using 100 - 20 noded brick elements (803 nodes). Predictor corrector form of Newmark Constant Average Acceleration Method (using Newton Raphson Scheme) has been used for solution of nonlinear dynamic equilibrium equations. The time step size has been kept equal to 0.5e-02 second in the time integration scheme to achieve the desired accuracy. Maximum number of iterations required to achieve convergence (forced balance type of

Table 1 Material properties for the reinforced concrete shell

Properties		Concrete	Steel
1	Modulus of Elasticity (MPa)	30000.0	200000.0
2	Poisson's Ratio	0.17	0.0
3	Ultimate Strain	0.0035	-
4	Compressive Strength (MPa)	35.0	460.0
5	Cracking Strain	$1.5 \times 10^{-4}$	-
6	Area Ratio of steel and concrete	0.026 (both direction)	-
7	Constants for fluidity parameter	$c_0 = -0.533172$ , $c_1 = 0.880166$	$a_0 = 1.539$ , $a_1 = 0.971$
8	Coefficients in dynamic strength equation ( $A_0, A_1, A_2$ )	1.48, 0.16, 0.0135	

criteria) in the analysis is 50. Material properties are given in the Table 1.

The objective of the study is to predict response of nuclear containment shell for transient pressure loading of a Phantom aircraft and blast loading of different amounts of blast charges at varying distances and compare the responses. The loading-time function for the Phantom aircraft as obtained from literature (Cervera *et al.* 1987) is shown in Fig. 1(b). The peak value of the impact load is 115 MN and the total impact duration is 0.073 sec. The above loading is applied to an area of 28 m<sup>2</sup>. An algorithm and software has been developed for calculation of blast pressures on a cylindrical shell and blast pressure calculation has been made using this software. Blast pressures on the shell surface vary depending upon the angle of incidence. The blast pressures have been calculated at the centre of the outer surface of brick elements. On the rear face of the shell with respect to blast direction only small pressure is exerted because of the large dimension of the structure. The wave front for the surface blast has been assumed to be a plane and therefore, there will be no variation in blast pressure along the height. The variation of the blast pressures for 20 t

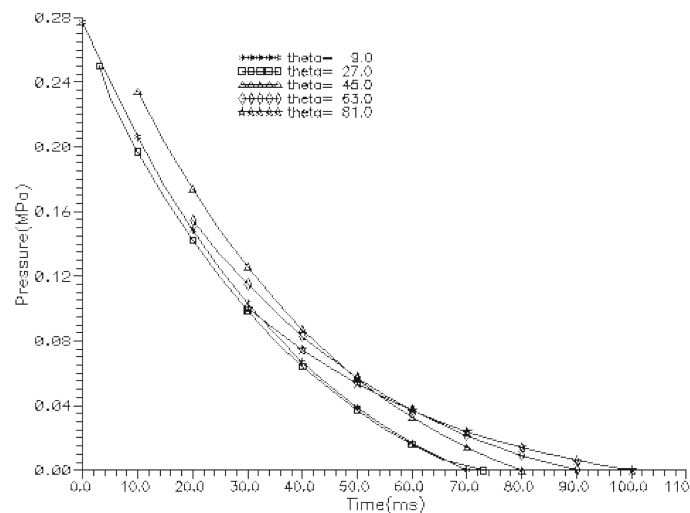


Fig. 3(a) Variation of blast pressure with time at different angles on the shell for blast of 20 t TNT at 100 m distance

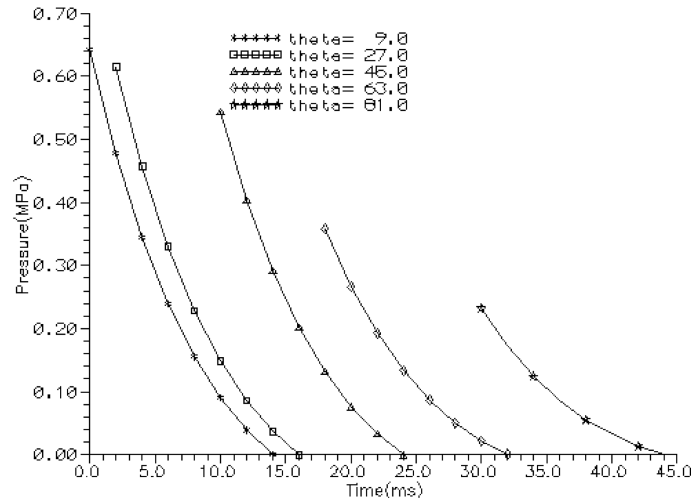


Fig. 3(b) Variation of blast pressure with time at different angles on the shell for blast of 0.5 t TNT at 20 m distance

surface blast load at a detonation distance of 100 m, at different angles of incidence with time is shown in Fig. 3(a) and the elements (centroid) lying at respective angles has been subjected to these pressure time histories. For this surface blast load of 20 t TNT at a detonation distance of 100 m, the positive phase duration is 70 ms and behaviour of the shell is dynamic. Only positive phase pressures have been considered in the analysis. The peak pressure value for blast of 20 t TNT is 0.277 MPa. The shell has also been analyzed for a surface blast load of 0.500 t at a distance of 20 m (close range). The positive phase duration of the blast wave is 14 ms for close range. The variation of the blast pressure at different angles with time is shown in Fig. 3(b) for blasts of 0.50 t TNT and the elements (centroid) lying at these angles has been subjected to these pressure time histories.

### 3.1 Deflections

Table 2 shows the peak deflections and the time of their occurrence for the impact of Phantom Aircraft and for two surface blast charges from close and long range. It is seen from the Table 2 that the peak deflection for impact of phantom aircraft is 50.55 mm at impact location itself. The peak deflection is 58.78 mm for the detonation of 0.500 t TNT at close range and 91.8 mm for the detonation of 20.0 t TNT at a longer range and in both of these cases the peak deflection occurs at

Table 2 Peak deflection for impact of aircraft & detonation of different surface blast charges

Description of Loading	Impact of Phantom Aircraft (Dynamic)	Close Range (Impulsive) $D = 20$ m 0.5 t TNT	Long Range (Dynamic) $D = 100$ m 20.0 t TNT
Peak Deflection (mm)	50.55	58.78	91.8
Time of Peak Deflection (sec.)	0.063	0.094	0.105

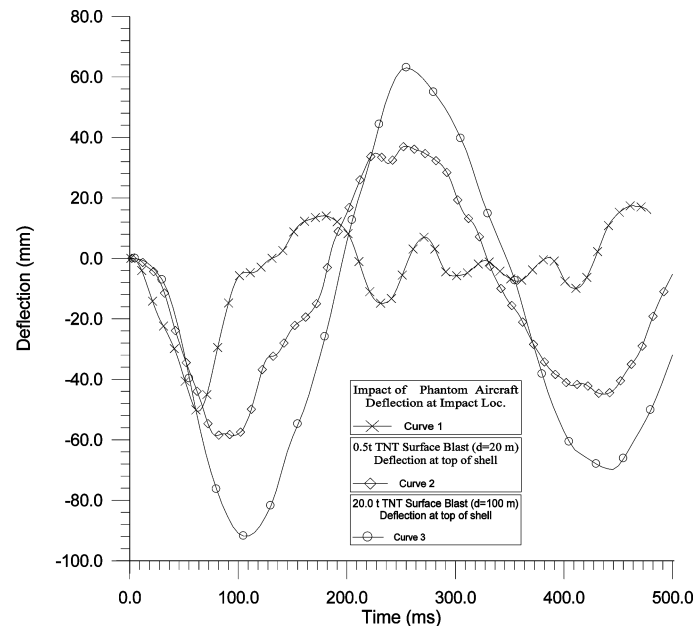


Fig. 4 Variation of deflection with time for impact of Phantom aircraft and surface detonation of different blast charges

top of the shell. The variation of deflections with time for impact of aircraft (Point A impact location) and for the detonation of two surface blast charges (20 t TNT at 100 m, 0.5 t TNT at 20 m) at the top of the nuclear containment shell (Point B, Fig. 1(a)) are shown in Fig. 4. It is seen from the figure that with an increase in the amount of the blast charge non-linear effects are higher and the time period of vibration increases, elongation in period of vibration is least in case of Impact of Aircraft as number of cracked gauss points is much less compared to other two cases. It is also observed that blast pressure for impulsive charge (0.5 t TNT at 20 m) is much more than the dynamic charge (20 t TNT at 100 m), however deflection is more in the case of blast of the dynamic charge (20 t TNT at 100 m).

### 3.2 Compressive stress in concrete

Table 3 shows peak value of the compressive stress (meridional and hoop) in concrete for Impact of Phantom Aircraft and for two surface blast charges from close and long range. The peak

Table 3 Peak compressive stress for different surface blast charges

Description of Loading	Impact of Phantom Aircraft (Dynamic)	Close Range (Impulsive) $D = 20$ m 0.5 t TNT	Long Range (Dynamic) $D = 100$ m 20.0 t TNT
Peak Stress in vertical direction (MPa)	-39.45	-19.68	-25.90
Stress in hoop Direction (MPa)	-38.70	-8.50	-4.90
Time at which peak Occurs (sec)	0.059	0.028	0.045

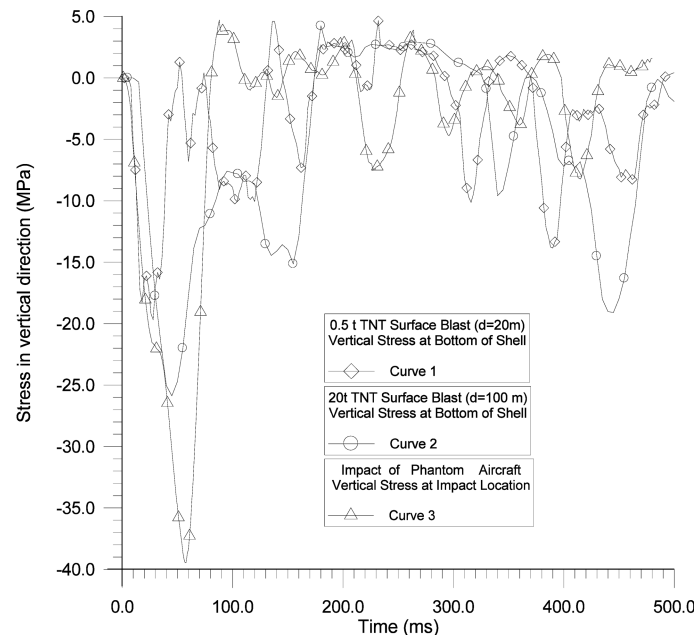


Fig. 5 Variation of Stress with time for impact of Phantom aircraft and surface detonation of different blast charges

compressive stress in the concrete occurs at the impact zone in concrete and the value is 39.45 MPa (this value is more than the static compressive strength however lesser than the dynamic compressive strength). As seen from the Table 3 the values of compressive stress obtained for detonation of surface blast charge at long range and close range is 25.9 and 19.68 MPa respectively and these values are lesser than the value obtained for the impact loading. Hoop stress is much more for impact of Phantom Aircraft compared to blast charges for close and long range. The values of stress in meridional (vertical) and hoop direction for impact and blast loading indicates that bending behaviour is predominant in case of blast and shell action is predominant in case of impact loading.

The variation of vertical stress (meridional) in concrete with time at a Gauss Point at the impact location (where peak occurs) and at bottom of the shell (El shown in Fig. 6) for detonation of blast charge of 0.5 t and 20 t TNT is shown in Fig. 5. It is observed that vertical (meridional) stress reaches its maximum value immediately with the application of the blast pressure possibly because of peak pressure in case of blast loading occurs instantly and in case of impact of Phantom Aircraft peak pressure occurs between 42 to 56 ms. The peak compressive stress is more in case of dynamic charge (20 t TNT,  $d = 100$  m) implying that it has more damage potential compared to impulsive charge (0.5 t TNT,  $d = 20$  m).

### 3.3 Crack pattern

For impact of phantom aircraft, the total cracked gauss points in one direction and two directions are 29.8 and 4.7 percent respectively. For detonation of blast charge of 20.0 t, 93.4% of the gauss points are cracked in one direction 70.1% gauss points are cracked in two directions. Similarly It is

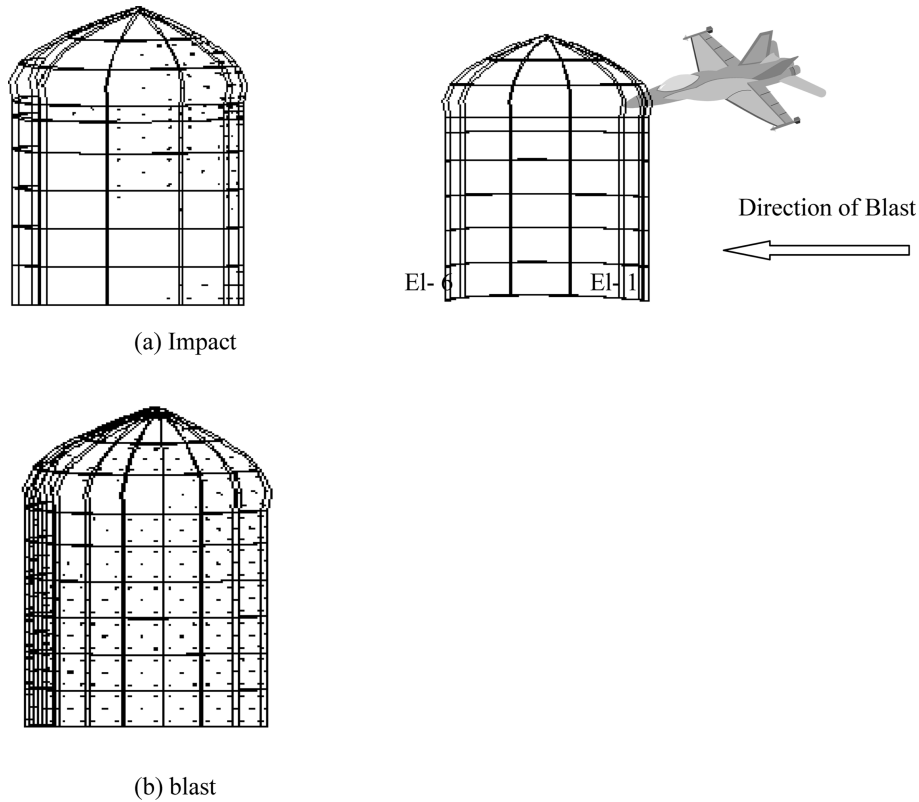


Fig. 6 Distribution of cracks for impact of Phantom aircraft and blast of 20.0 t TNT at a distance of 100 m from nuclear containment shell

found that for surface detonation of 0.5 t TNT charge, 99.0%, gauss points are cracked in one direction and 73.0% gauss points are cracked in two directions.

### 3.4 Yielding and failure of concrete

During the impact process, a large number of gauss points have reached the yield surface and a few of them have reached the failure surface as obtained by the proposed failure criterion. For a cracking strain of 0.00015, five gauss points reached the failure curve, three of which are in the close vicinity of the impact zone and two are at the top of the dome. A large number of Gauss

Table 4 Number of G.P. crossed failure surface

Description of Loading	Impact of Phantom Aircraft (Dynamic)	Close Range (Impulsive) $D = 20$ m 0.5 t TNT	Long Range (Dynamic) $D = 100$ m 20.0 t TNT
No. of Gauss Points Reached or Crossed the Failure Surface	5	36	16

Points crossed the yield surface for all the three blast charges considered in the study and a few of them crossed the failure surface for higher blast charge as seen in Table 4.

### 3.5 Stress in reinforcement

The peak value of tensile stress at the reinforcement is 294 MPa for impact of Phantom aircraft. The peak tensile stress is 314 MPa for blast of 20.0 t ( $d = 100$  m), 196 MPa for blast of 0.5 t ( $d = 20$  m) charge.

## 4. Discussion of response for impact and blast loading

The magnitude, engulfed area and duration of pressure loading in case of impact and blast are different. The impact of an aircraft (Phantom) produces intense pressure loading (peak pressure being 4.1 MPa) acting in a relatively very small area (0.63% of the front face). The pressure loading obtained from the analysis in the case of blast (close and long range) is relatively much smaller (0.63 MPa for near blast and 0.27 MPa for blast from long range) but much larger surface areas are pressurized. Table 5 shows details of pressure loading and % engulfed area of the containment shell. It is seen from the table that 60% of the front face in case of nearby blast for a duration of 11.75-14 ms and 100% of front face for a duration of 29-70 ms in case of blast from long range is pressurized.

The loading produced in the impact of an aircraft and blast from long range (20 t TNT,  $d = 100$  m) is dynamic in nature for nuclear containment shell as fundamental time period for the shell is 220 ms and duration of the loading in case of impact is 73 ms (Fig. 1(b)) and duration of loading for blast from long range is 70 ms (Fig. 3(a)). Blast loading is impulsive for the containment shell for small charge at near range (0.5 t TNT,  $d = 20$  m) for which positive phase duration is 14 ms (Fig. 3(b)).

Table 5 Details of pressure loading and % engulfed area of the containment

Impulsive Blast (0.5 t, $d = 20$ m) (Close Range)		Dynamic Blast (20.0 t, $d = 100$ m) (Long Range)	
Time Interval (ms)	% Area of front face engulfed with shock pressure	Time Interval	% Area of front face engulfed with shock pressure
0.0 - 4.5	20	0.0 - 3.0	20
4.5 - 11.7	40	3.0 - 10.0	40
11.7 - 14.0	60	10.0 - 18.0	60
14.0 - 22.0	40	18.0 - 29.0	80
22.0 - 28.0	40	29.0 - 70.0	100
28.0 - 34.0	40	70.0 - 73.0	80
34.0 - 36.0	40	73.0 - 80.0	60
36.0 - 40.0	40	80.0 - 88.0	40
40.0 - 48.0	20	88.0 - 99.0	20

The nature of deflection of containment shell is different in case of impact and blast for the nuclear containment shell. The peak deflection in case of impact is at the impact location however in case of blast loading the peak deflection is at the top of the nuclear containment shell. Variation of deflection with time for impact of Phantom aircraft and blast at near and long range (Fig. 4) indicate that the static component is more in case of impact. The increase in time period because of nonlinear material modeling and cracking is highest in case of blast from bigger charge from long range (20.0 t TNT,  $d = 100$  m). The deflection with time response for impact of Phantom aircraft and blast (20.0 t TNT,  $d = 100$  m and 0.5 t TNT,  $d = 20$  m) show that elongated period varies from 250 ms in case of impact to 330 ms for blast from close range and 358 ms for blast from long range. For the two cases of blast considered, it is found that in the near range blast creates impulsive response and the number of cracks being more compared to long range blast which creates dynamic response. It is found that elongation in the period as well peak deflection is more in the case of blast from long range as the duration of loading being less in case of impulsive loading the cracks gets closed earlier.

The percentage cracked gauss points in one direction being 29.75% in the impact and it is more than 90 percent in the case of blast loading (close and long range) which may elongate the period however, the peak stress in concrete is more in the case of impact from an aircraft. The cracking pattern for impact of phantom aircraft and blast of long range (20 t TNT,  $d = 100$  m) is shown in Fig. 6, it is seen from the figure that the cracks in case of impact or mostly at impact location however the cracks in case of blast loading is distributed throughout the structure.

## 5. Conclusions

Following are the conclusions drawn from the study.

(i) The intense compressive stresses in both vertical and hoop direction are created for impact of Phantom Aircraft at impact location. The peak compressive stress in case of the blast for long range and close range in vertical direction occurs at bottom of the shell and magnitude is lesser by 34.3%, 50.1% respectively compared to impact of Phantom Aircraft and hoop stress is appreciably low in both the cases at this location compared to impact of an aircraft. The analysis of stresses indicated that bending behaviour is predominant in response of the shell subjected to blast loading, however in case of impact of aircraft the shell action is predominant (hoop and meridional stresses are of the same magnitude).

(ii) The behaviour of containment shell under impact of various aircrafts is dynamic as the impact duration for various aircraft (Abbas *et al.* 1995, Kukreja 2005) are more compared to Phantom Aircraft however in case of blast loading the behaviour is dynamic or impulsive depending upon the amounts of charge and detonation distance.

(iii) Aircraft impact loading is a localized phenomenon as most of the cracks occur in the vicinity of the impact location, whereas, in the case of blast loading, most of the cracks are distributed throughout the structure with greater percentage of the total cracked gauss points. Peak deflection in case of aircraft impact occurs at the impact location itself, however in case of blast loading, peak deflection occurs at top of the shell.

(iv) The outer reinforced concrete shell of the containment structure is capable of withstanding the impact of the aircraft with a little localized damage (0.6% of associated volume where failure surface is crossed and material degradation began) in the vicinity of the impact location, however

the blast loading produced more damage and material degradation began at comparatively more locations (2.4% of associated volume failure surface is crossed). Sufficiently much more number of Gauss Points yielded in the blast loading compared to impact of the aircraft implying much more plastic deformation in the shell in the case of blast loading.

## References

- Abbas, H., Paul, D.K., Godbole, P.N. and Nayak, G.C. (1996), "Aircraft crash upon outer containment of nuclear power plant", *Nucl. Eng. Des.*, **160**, 13-50.
- Atchley, B.L. and Furr, H.L. (1967), "Strength and energy absorption capabilities of plain concrete under dynamic loads", *ACI J.*, **64**, 745-755.
- Bicanic, N. and Zienkiewicz, O.C. (1983), "Constitutive model for concrete under dynamic Loading", *Earthq. Eng. Struct. Dyn.*, **11**, 689-711.
- Bischoff, P.H. and Perry, S.H. (1991), "Compressive behavior of concrete at high strain rates", *Mater. Struct.*, **24**(4), 425-458.
- Cadoni, E., Labibes, K., Berra, M., Giangrasso, M. and Albertini, C. (2000), "High strain rate tensile behaviour of concrete", *Mag. Concrete Res.*, **52**(5), 365-370.
- Cervera, M., Hinton, E. and Bicanic, N. (1987), "Non-linear transient dynamic analysis of three dimensional structures", *Numerical Methods and Software for Dynamic Analysis of Plates and Shells*, Ed. Lewis, R.W., Pineridge Press, Swansea, U.K.
- Crutzen, Y., Reynue, J. and Vellafane, E. (1981), "Impulsive loading on concrete structures", SMIRT 6, Paper J, 10/1 Paris.
- Dilger, W.H., Koch, R. and Kowalczyk, R. (1984), "Ductility of plane and confined concrete under different strain rate", *ACI J.*, **81**(1), 73-81.
- Gong, S., Lu, Y., Tu, Z. and Jin, W. (2009), "Validation study on numerical simulation of RC response to close in blast with a fully coupled model", *Struct. Eng. Mech.*, **32**(2), 283-200.
- Gupta, A.K. and Maestrini, S.R. (1990), "Tension Stiffness model for reinforced concrete bars", *J. Struct. Eng.-ASCE*, **116**(3), 769-790.
- Hughes, B.P. and Gregory, R. (1972), "Concrete subjected to high rates of loading in compression", *Mag. Concrete Res.*, **24**(78), 25-37.
- Hughes, B.P. and Watson, A.J. (1978), "Compressive strength and ultimate strain of concrete under impact loading", *Mag. Concrete Res.*, **30**(105), 189-198.
- Kukreja, M. (2005), "Damage evaluation of 500 MWe Indian pressurized heavy water reactor nuclear containment for aircraft impact", *Nucl. Eng. Des.*, **235**, 1807-1817.
- Luccioni, B.M., Ambroshini, R.D. and Danesi, R.F. (2004), "Analysis of building collapse under blast loads", *Eng. Struct.*, **26**, 63-71.
- Mlakar, P.F., Corley, W.G., Sozen, M.A. and Thornton, C.H. (1999), "The Oklahoma city bombing, analysis of blast damage to Murrah Building", *J. Perform. Constr. Fac.*, **12**(3), 113-119.
- Menetrey, P. and Willam, K.J. (1995), "Tri-axial failure criterion for concrete and its generalization", *ACI Struct. J.*, **92**(3), 311-318.
- Ngo, T. and Mendis, P. (2009), "Modelling the dynamic response and failure modes of reinforced concrete structures subjected to blast and impact loading", *Struct. Eng. Mech.*, **32**(2), 269-282.
- Nilsson, L. and Glemberg, R. (1981), "A constitutive model for concrete in high rate of loading situations", *Proceedings of the IABSE*, Colliquim Delft.
- Omika, Y., Fukuzawa, E., Koshika, N., Morikawa, H. and Fukuda, R. (2005), "Structural response of world trade center under aircraft attacks", *J. Struct. Eng.-ASCE*, **131**(1), 6-15.
- Osteraas, J.D. (2006), "Murrah building bombing revisited : A qualitative assessment of blast damage and collapse patterns", *J. Perform. Constr. Fac.*, **20**(4), 330-335.
- Pandey, A.K., Kumar, R., Paul, D.K. and Trikha, D.N. (2006a), "Nonlinear response of reinforced concrete containment structure under blast loading", *Nucl. Eng. Des.*, **236**, 993-1002.

- Pandey, A.K., Kumar, R., Paul, D.K. and Trikha, D.N. (2006b), "Strain rate model for dynamic analysis of reinforced concrete structures", *J. Struct. Eng.-ASCE*, **132**(9), 1393-1401.
- Perzyna, P. (1966), "Fundamental problems in visco-plasticity", *Adv. Appl. Mech.*, **9**, 243-77.
- Rebora, B. and Zimmerman, T. (1976), "Dynamic rupture analysis of reinforced concrete shells", *Nucl. Eng. Des.*, **37**, 269-297.
- Ross, C.A., Tedesco, J.W. and Hughes, M.L. (1995), "Effects of strain rate on concrete strength", *ACI Mater. J.*, **92**(1), 37-47.
- Scott, B.D., Park, R. and Priestely, M.J.N. (1982), "Stress-strain behaviour of concrete confined by overlapping hoops at low and high strain rates", *ACI J.*, **79**(1), 13-27.
- Soroushian, P., Choi, K.B. and Alhamad, A. (1986), "Dynamic constitutive behavior of concrete", *ACI Struct. J.*, **83**(2), 251-259.
- Xiao, S., Li, H. and Lin, G. (2008), "Dynamic behaviour and constitutive model of concrete at different strain rates", *Mag. Concrete Res.*, **60**(4), 271-278.
- Yang, L. and Kai, X. (2004), "Modelling of dynamic behaviour of materials under blast loading", *Int. J. Solids Struct.*, **41**(1), 131-143.

## Notations

- $A_0, A_1, A_2$  : Constants in description of dynamic compressive strength
- $a_0, a_1$  : Constants in fluidity parameter equation for steel
- $c$  : Cohesion strength in the description of the failure criteria
- $c_0, c_1$  : Constants in fluidity parameter equation for concrete
- $e$  : Eccentricity parameters
- $f_{cd}$  : Dynamic compressive strength of concrete
- $f_c$  : Static compressive strength of concrete
- $f_t$  : Tensile strength of concrete
- $f_{sy}$  : Yield Strength of steel
- $F$  : Failure surface
- $G_o, G_c$  : Shear modulus of the un-cracked concrete and cracked concrete
- $I_1, J_2, J_3$  : Stress invariants
- $m$  : Friction parameter in the three dimension failure criterion
- $n$  : Modulus of Elasticity Ratio of steel and concrete
- $X_A, X_B, X_C$  :  $X$  Coordinates of the controlling points A, B, C for tension stiffening curve
- $Y_A, Y_B, Y_C$  :  $Y$  Coordinates of the controlling points A, B, C for tension stiffening curve
- $\beta$  : Reduction factor for shear modulus
- $\gamma$  : Fluidity parameter
- $\varepsilon_{ij}$  : Strain tensor
- $\varepsilon^p$  : Viscoplastic strain tensor
- $\dot{\varepsilon}_{ef}$  : Effective strain rate
- $\phi(F)$  : A function of failure surface
- $\sigma_{ij}$  : Stress vector
- $\theta$  : Angle of similarity in failure criteria
- $\xi$  : A function of first stress invariants
- $\sigma_y$  : Initial yield stress of concrete
- $r(\theta)$  : An elliptic function for three dimensional failure criterion
- $\rho$  : A function of second stress invariant
- $\rho_a$  : Area ratio of the reinforcement and concrete